Granular Matter (2019) 21:34
https://doi.org/10.1007/s10035-019-0888-4

ORIGINAL PAPER

Characterization of aggregation and declustering tendency of hydrophobic fine particles in water

Berrin Tansel[1] · **Daria Boglaienko**[1]

Received: 27 August 2018 / Published online: 25 March 2019

Abstract
When hydrophobic particles are added to water, they form clusters by interparticle gas bridging. The hydrostatic, capillary and buoyancy forces acting on the submerged clusters can gradually mobilize the interparticle gas bubbles. As particles are released from the cluster gradually, the cluster is transformed into slurry state. We studied the clustering and declustering characteristics of hydrophobic granular particles (dyed quartz sand with 0.33 mm and 0.73 mm in diameter), which were applied to the water surface and submerged after forming clusters. Behavior of the particle clusters was evaluated to characterize (1) clustering tendency of particles, and (2) gradual particle declustering by mobilization, coalescence and release of air bubbles from the submerged cluster. Cluster formation and declustering rates of the particles were evaluated based on the experimental data and observations. Clustering tendency of the particles depends on the surface tension characteristics (or spreading tendency) of the particles on the water surface. On the other hand, stability of the submerged cluster is highly dependent on the surface roughness which we propose affects the ability of the microbubbles to coalesce within the submerged cluster. Particle cohesion coefficient for clustering tendency and particle declustering rate for transformation of the submerged aggregate to slurry state were estimated from experimental data.

Keywords Hydrophobic particles · Granular clusters · Cassie state · Hydrophobic surfaces · Particle declustering · Microbubble bridging

1 Introduction

Spontaneous attachment of micro bubbles occur on hydrophobic surfaces when they are submerged in liquids. Under submerged conditions, hydrophobic surfaces are attracted to each other via bridging of the gas bubbles [6, 15]. As a result, the interfacial bubbles that form at the liquid–solid interfaces create adhesive forces that can hold small particles in cluster form for extended periods of time under submerged conditions [1, 2, 4, 15, 23].

Although the shapes and stability limits of the capillary liquid bridges that form by liquid entrapment between two solid surfaces have been studied extensively [7, 13, 17–21, 24, 30]; there is very limited understanding of the capillary gas bridges that form by gas bubbles entrapped between solid surfaces that are submerged in liquids. Even for the case of capillary cohesion by liquid bridges, the theories developed are based on two dimensional scenarios with only two particles interacting. Particle clusters in water form three dimensional aggregates and include numerous particles which are held together by interparticle capillary gas bubbles. The hydrostatic, capillary and buoyancy forces acting on the submerged particle clusters can result in gradual mobilization, coalescence and release of the gas bubbles which occurs simultaneously with the declustering process over time.

The theories developed for macroscale bubble behavior (e.g., Young's equation) are not applicable at the smaller scales (nanoscale and micro) as other phenomena come into play (e.g., line tension, surface forces, surface roughness) [6, 22]. In contrast to the adhesive forces by capillary liquid bridges, the compressibility of the capillary gas bridges is a function of the pressure effects on the adhesive forces [5]. Numerical analyses to estimate the adhesive forces of the gas bridges show a direct correlation between the particle radius, surface energy of the liquid gas interface,

✉ Berrin Tansel
tanselb@fiu.edu

[1] Civil and Environmental Engineering Department, Engineering Center, Florida International University, 10555 West Flagler Street, Miami, FL 33174, USA

macroscopic contact angle and the adhesive force [5]. In addition, the contact angle between the gas and the solid phases is not comparable to the inverse wetting angle as defined by the Young equation. Theoretical analyses show that contact angle is a function of both the surface energies and the system geometry [5].

Super hydrophobicity occurs on surfaces of topography with protrusions or roughness grooves. Such rough surfaces can entrap air (gas bubbles) in grooves, hence, exhibit super hydrophobic characteristics such that when a water drop comes into contact with the surface, water does not spread or penetrate into the surface topography. As a result, the water drop forms a high contact angle and can roll on the surface [8, 11, 16]. In this case wetting regime can be characterized by Cassie theory, as described by the following equation:

$$\cos\ \theta^* = f_1 \cos\ \theta - f_2 \quad (1)$$

where $\cos\theta^*$ is the apparent contact angle; f_1 and f_2 are the areas of solid/liquid and air/liquid interface per unit projected surface area, respectively; θ is the intrinsic contact angle for a flat surface [8]. This equation shows that the lower wetting conditions result in higher contact angle (and larger f_2). Hence, the larger the area covered by the gas phase (or air bubbles), the more likely the super hydrophobic regime will occur. Development of interfacial air bubbles on granular surfaces increases the stability of the hydrophobic cluster. Conversely, release of an air bubbles would lead to enhanced wetting and destabilization of the particle cluster.

Interfacial bubbles, particularly micro and nanobubbles, that form at the liquid–solid interfaces provide an explanation for the attraction between hydrophobic surfaces [4, 15, 21, 23], adhesion of colloidal particles [1, 2], and facilitation of attachment of macroscopic bubbles on solid surfaces [12, 28]. Hydrophobic surfaces remain attached to each other via bridging of micro and nanobubbles [15], or, in other words, due to capillary gas phase bridging caused by micro and nanobubbles [6]. The capillary gas phase bridging force is comprised of surface tension (between three phases) and Laplace pressure difference across the curved interface.

Three phase contact stability of bubbles in relation to bubble size has been studied extensively. It had been observed that bubbles of colloidal size ranging from 10 to100 nm radii are very unstable with lifetimes ranging from about 1 to 100 µs, whereas bubbles of millimeter size range can live for months [9]. Experimental studies have also reported existence of nanobubbles with longer lifetimes (a few hours) that contradicts the Laplace pressure conditions [25, 27]. One explanation for the longer lifetime of a nanobubble is the larger contact angle and bubble elongation (larger radius) which decreases the Laplace pressure inside of the bubble [26]. Another explanation is that there is a film of contaminant at air–water interface that decreases contact angle [4]. A third explanation for the long lifetimes of the interfacial nanobubbles is based on the pinned three-phase boundary of the nanobubbles [29].

Determination of wetting characteristics of the hydrophobic surfaces involves application of a water drop to the hydrophobic surface and measuring the wetting angle. However, this method is not suitable to study the wetting characteristics of hydrophobic particle clusters that form in liquids due to entrapment of air bubbles within the cluster which changes the wetting characteristics. Such particle clusters form in the environment by interaction of oil contaminated sand particles with water. When submerged in water, these hydrophobic particle clusters can remain intact for extended periods of time (e.g., tar balls forming after oil spills). Similar clustering phenomenon occurs when hydrophobic particles are added directly to water (creating particle aggregates). Evaluation of the three dimensional particles and entrapped gas phase which form clusters is often explained by representations using only two interacting particles [17, 30]. However, these studies neither provide insight for the clustering tendency of the particles during interaction with water phase nor declustering rate of submerged aggregates in water that are important characteristics for field and industrial applications (e.g., cement mixing).

We studied the particle-liquid-gas interactions by directly applying the hydrophobic particles to the water surface until they submerged by forming a cluster. We evaluated the submergence, clustering, and declustering behavior of hydrophobic sand particles (0.33 mm and 0.73 mm) in view of (1) clustering tendency, and (2) microbubble coalescence and declustering process (i.e., transformation rate of the submerged cluster to slurry state).

2 Materials and methods

Experiments were performed to determine the effect of particle size on the initial clustering and submergence characteristics of particle on the water surface, and declustering of particles from the submerged cluster. Dyed quartz sand particles (brown and green) were used as the hydrophobic granular materials (Fig. 1a). Table 1 presents the characteristics of the hydrophobic particles used. Brown sand (quartz) was obtained from Ashland (Irving, TX; decorative stone granules) and green sand (quartz) was obtained from Activa products (Marshall, TX).

Initially, the granular materials were sieved to separate into three size groups for each sand type. The granular particles were sieved using standard sieves to separate particles with specific sizes to ensure uniform particle size. After sieving, the green sand was separated into three particle sizes with average particle diameters of 0.150, 0.180, and 0.250 mm; and the brown sand was also separated into three sizes with average particle diameters of 0.425, 0.600,

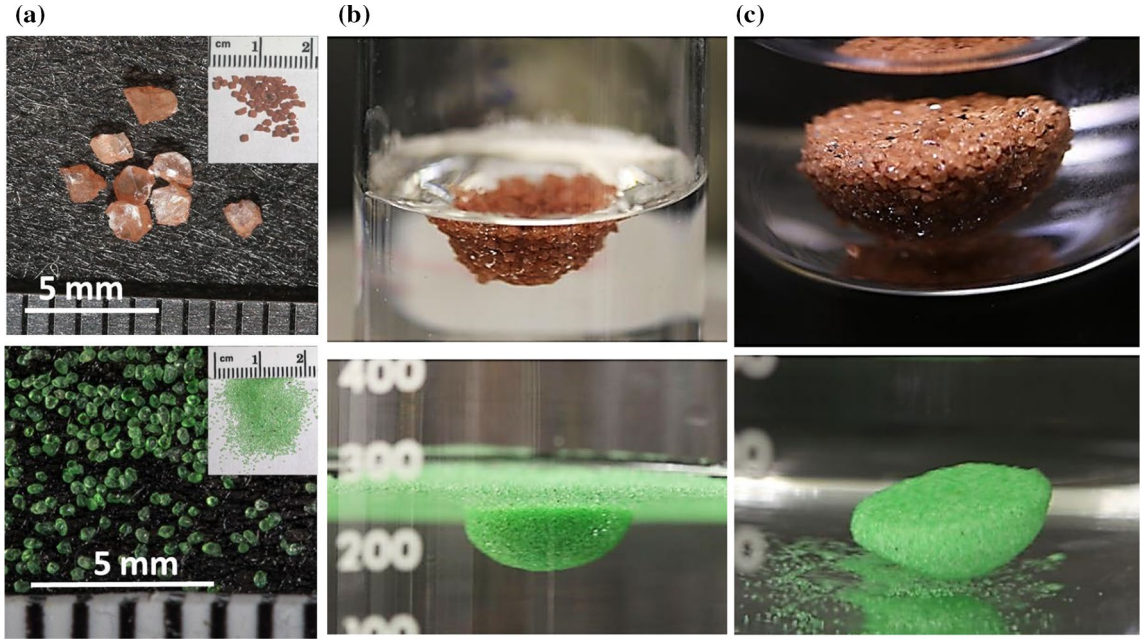

Fig. 1 Formation of granular clusters in water: **a** granular particles used, **b** granular cluster formation, **c** submerged particle clusters in water. Air microbubbles are visible on the brown sand particles of the cluster submerged in water

Table 1 Characteristics of the granular particles used

Parameter	Notation/determination	Green sand	Brown sand
Particle size range	Based on sieve sizes	$(2.50-4.20)\times10^{-4}$ m	$(5.95-8.41)\times10^{-4}$ m
Particle size (average)	d_p	3.30×10^{-4} m	7.30×10^{-4} m
Average particle radius	r_p	1.65×10^{-4} m	3.65×10^{-4} m
Bulk density	Measured	1550 kg/m^3	1700 kg/m^3
Average particle weight	m_p g	2.51×10^{-6} N	2.71×10^{-5} N
Shape	Visual examination	Round	Angular
Surface characteristics	Visual and microscopic examination	Smooth	Rough

and 0.850 mm. The stated average particle diameters are the middle values between the sieve sizes used.

Preliminary experiments conducted did not show a significant difference in terms of cluster formation and declustering behavior between the different size particles for each type of sand. However, there were significant differences between the two types of sand (green and brown) used. Therefore, detailed analyses were conducted using one size granular particles for each sand type. For the experiments, granular materials were classified by sieving using standard sieves No. 20 and 30 for the brown sand and No. 40 and 60 for the green sand by using the material captured between the two sieves indicated. After sieving, the brown sand had particle size range <0.841 mm and >0.595 mm and bulk density of 1.70 g/cm^3, and the green sand had particle size range <0.420 mm and >0.250 mm and bulk density of 1.55 g/cm^3. Cluster submergence experiments were performed with deionized water at room temperature (22 °C).

Hydrophobic particles were added gently (i.e., free flow from a paper tray by slowly tilting the tray) to the water surface from a distance of 5 cm and remained floating, while clustering in the area of application radius. To determine the weight of the cluster at the time of submergence, a 50-mL beaker was placed on an electronic balance to record the amount of the particles applied. When the aggregate started to submerge (due to the weight of the floating granular aggregate exceeding the forces that made the aggregate stay afloat, i.e., buoyancy and surface tension of water), the total amount of the granular material applied was recorded (Fig. 1b, c). Surface composition of the granular materials were analyzed using JEOL 6330F field emission scanning electron microscopy (FEG-SEM) with energy dispersive spectroscopy (EDS) thermo.

3 Results and discussion

Examination of the SEM images as well as visual inspection of the green and brown sand particles showed significant differences in the surface characteristics. The brown sand particles had rough surfaces with sharp edges while green sand particles were round with smooth surfaces (Fig. 1a). Brown sand surface consisted of primarily carbon (41.72%), oxygen (34.00%), silicon (19.06%), aluminum (2.82%), potassium (1.30%) and sodium (1.11%). Green sand consisted of carbon (37.85%), oxygen (34.98%), silicon (24.62%), aluminum (0.56%), and chlorine (1.98%). Surface composition variations are due to presence of dye on the sand particles.

Surface tension of the water allowed the hydrophobic sand particles to remain afloat on the water surface while forming an aggregate. The floating aggregate had relatively large quantities of completely dry particles (Fig. 1b and Fig. 2a). With the addition of particles (i.e., increased gravitational force), the floating particle aggregate submerged as a large cluster without breaking (Fig. 1c). The submerged particle clusters retained their shape, likely due to the hydrophobic nature of the particles that caused the air to be entrapped between the particles (Cassie wetting regime). The entrapped air resulted in formation of a hydrophobic interface for the aggregate after it was submerged in water (Fig. 1c). Air bubbles could be seen by naked eye on the submerged particle clusters, especially in the submerged brown sand clusters (Fig. 2b). Similar phenomena have been described by Nguyen et al. [14] during their investigations of the stability of the powder-liquid interface of the liquid marbles using hydrophobic silica powder for the marble's shell, or encapsulation. The silica powder particles were observed to be positioned at the air–liquid interface at a distance from each other which prevented the inner liquid phase from contact with the outer wetting surface (Fig. 3a). Stability of the marble's hydrophobic surface was also related to the Cassie and Baxter model. Even though the observations by Nguyen et al. [14] were made for the encapsulated liquid drop exposed to air (case in Fig. 3a), which is the opposite of our case (i.e., submerged aggregate in water with air as the inner phase) (case in Fig. 3b). In both cases, hydrophobic particles provided a barrier that prevented the liquid from moving through the particles.

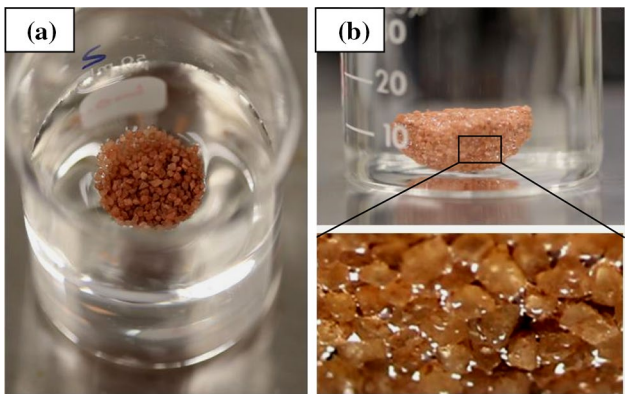

Fig. 2 Bubble entrapment in clusters. **a** Dry particles accumulating at the center in the floating cluster, **b** Visible air bubbles in the submerged cluster

4 Clustering tendency of granular particles

The mass of granular particles added to the water surface until the submergence of the floating aggregate was almost constant with the brown sand particles. However, for the green sand particles (which were smaller than the brown sand), the amount of sand added increased with decreasing particle size until the floating aggregate submerged. It was also noted that the green sand particles dispersed on the water surface forming a floating dispersed particle layer while the larger brown sand particles exhibited very little

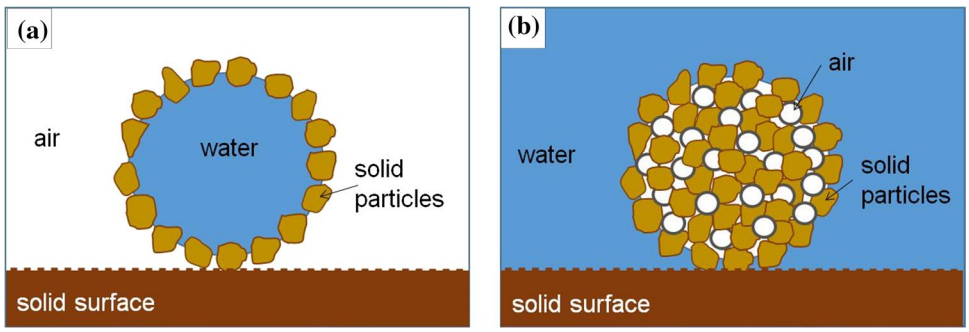

Fig. 3 Particles at air–water and water–air interface. **a** Particles at air–water interface: Hydrophobic solid particles remain attached at the air–water interface of a water drop, preventing its interaction with the surrounding air phase and from wetting the solid surface at the bottom. **b** Particles at water–air interface: Air bubbles on hydrophobic solid particles remain attached to the solid surface and result in formation of large particle clusters; hence, preventing the interaction of the cluster with the surrounding water phase

dispersion on the water surface. The larger amount of floating residual particles remaining on the water surface may have contributed the increased mass recorded with smaller particle sizes for the green sand. However, when this error was corrected, there was still a distinct difference in the mass of the submerged green sand aggregates (Fig. 4a).

Based on the definition of surface tension (force per unit length), surface tension of water (γ_{vl}) can be written in terms of cluster mass (m_c), gravitational constant (g), and cluster radius (R_c) as follows:

$$\gamma_{vl} = \left(m_c\, g\right) / 2\pi R_c \tag{2}$$

$$R_c = \left(m_c\, g\right) / \left(2\pi \gamma_{vl}\right) \tag{3}$$

There was some scatter in the data for the green sand particles for the ratio of experimentally measured cluster weight to experimentally measured cluster perimeter (Fig. 4c) due to the scattering of the smaller green and particles on the water surface in comparison to the larger brown sand particles. The experimentally measured cluster radius (R_{cm}) was significantly smaller (0.013 m for green sand, 0.0012 m for brown sand) than the values obtained from the Eq. (3) (0.124 m or 9.57 times larger for green sand, 0.102 m or 8.49 times larger for brown sand) (Fig. 4b). This deviation may be caused by the stretching of the water surface (in the shape of a sac) that allowed the particles accumulate both vertically and horizontally on the water surface (Fig. 1b). By assuming the particle sac forming on the water surface is in the shape of a half sphere (Fig. 1b), by flattening the area of the half sphere to a circle (i.e., flat water surface) with the same area, it was calculated that the corresponding cluster radius would be 2π times larger (or 8.79 times) than the observed cluster radius. This increase in the cluster radius (2π or 8.79 times) is comparable to the calculated cluster radius (9.57 times larger for green sand, 8.49 times larger for brown sand) using on the experimentally determined cluster mass in Eq. 3.

The formation of particle sac on the water surface indicates that particle–particle cohesion forces were stronger in comparison to the particle-water forces that allowed the water surface to stretch. The particle cohesion coefficient (P_{cc}) for the floating particle aggregate was defined as a measure of the clustering tendency of particles (i.e., tendency to form a floating particle sac) on the water surface as follows:

$$P_{cc} = R_c / R_{cm} \tag{4}$$

which can be estimated from the experimental data. By inserting the value of R_c from the Eq. (3) into the Eq. (4):

$$P_{cc} = \left(m_c\, g\right) / \left(2\pi\, R_{cm} \gamma_{vl}\right) \tag{5}$$

This is essentially the ratio of forces pulling the aggregate together to the interfacial tension of water (Fig. 5):

$$P_{cc} = \left(\gamma_{sv} + \gamma_{sl} \cos\theta\right) / \gamma_{vl} \tag{6}$$

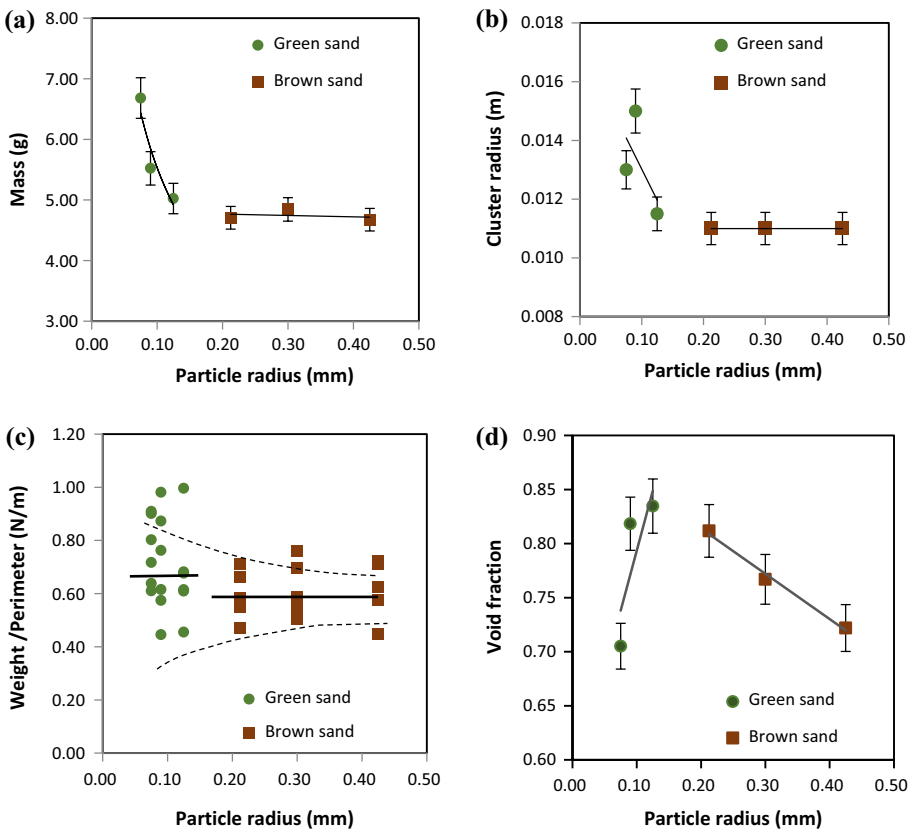

Fig. 4 Experimentally determined characteristics of the granular clusters formed on water surface before submergence. **a** Mass of particles added until submergence, **b** Maximum cluster diameter before submergence, **c** Weight per unit perimeter of the cluster on water surface (i.e., perimeter of the floating cluster, not considering the particles that were floating but not associated with the cluster), **d** Void fraction in the submerged cluster

The estimated particle cohesion coefficient (P_{cc}) for the floating clusters sand (9.57 and 8.49 for green and brown, respectively) indicate that both green and brown sand particles were hydrophobic and green sand particles had relatively higher tendency to aggregate on the water surface in comparison to the brown sand particles.

5 Packing density and void ratio of submerged clusters

Stability of clusters can be affected by the packing density of sand particles or void ratio. The submerged clusters with high void ratios have lower stability and decluster faster. We estimated the void ratio as follows:

$$\varepsilon = \frac{Vc - Vp}{Vp} \tag{7}$$

where ε is the void ratio, v_c is the volume of cluster, v_p total volume of particles in the cluster. The total volume of particles in the cluster (v_p) was estimated by multiplying the number of particles in the cluster and the average volume of one particle. The number of particles in the submerged cluster was estimated gravimetrically. The results showed that void fractions of the brown sand cluster decreased with increasing particle size (for particle sizes 0.425, 0.60, 0.85 mm). However, there the void fractions for the green sand clusters increased in relation to particle size (for the particle sizes 0.15, 0.18, 0.25 mm). The green sand particles had round shapes and smooth surfaces (Fig. 1a) that allowed a different packing arrangement in comparison to the brown sand particles which had irregular shapes and rough surfaces. The estimated void fractions of the submerged particle clusters ranged from about 0.7 to 0.8 which indicate very loose random packing for both green sand and brown sand clusters (Fig. 4d).

6 Microbubble coalescence and declustering of submerged clusters

In this study, formation and stability of the particle clusters were analyzed for the following interactions: (1) clustering of the hydrophobic particles (by interparticle gas bridging), and (2) gradual particle declustering by creep coalescence of interparticle gas phase and release of air bubbles from the submerged cluster. We observed that after submergence, air bubbles that were entrapped within the particle clusters began slowly coalescing to form a larger air pocket within the cluster. Especially with the larger particles (brown sand), formation of small cracks on the cluster surface (cluster-water interface) were visible. Gradually, a large air bubble (4–6 mm) was released from the top of the submerged aggregate (generally at the highest point of the aggregate) (Fig. 6). Simultaneously with the bubble coalescence process, some particles detached from the cluster. Multiple air bubbles were released over time at about equal time intervals. During this process, the particles in the cluster slowly detached, eventually forming a pile of loose particles (Fig. 6a) (i.e., slurry state). However, the very last air bubble released from the clusters was significantly different both in size, appearance, and behavior. For the brown sand, the last bubble was

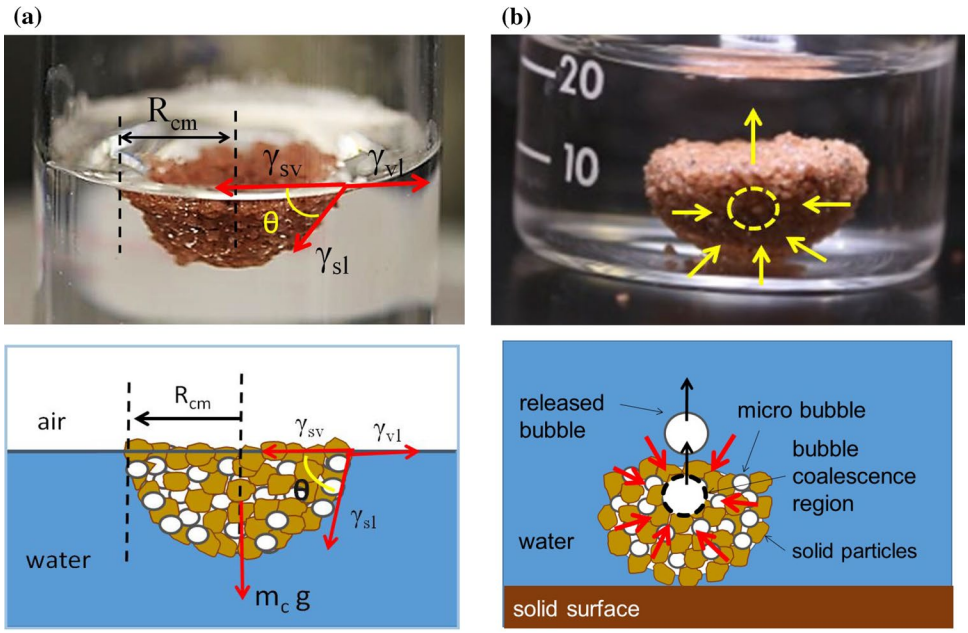

Fig. 5 Description of particle clusters for numerical analyses. **a** Interfacial effects on the floating cluster, **b** Bubble coalescence in the submerged cluster

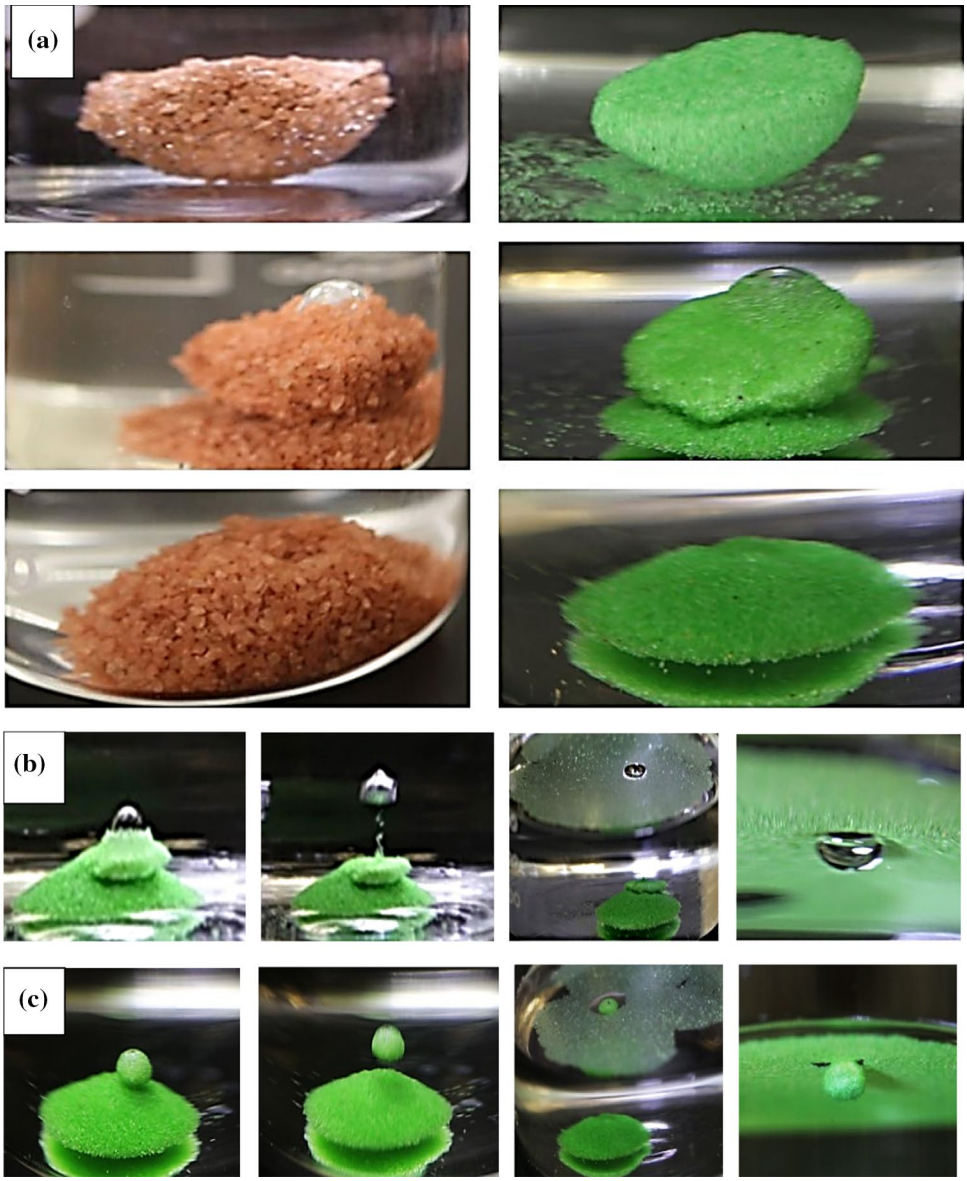

Fig. 6 Release of large gas bubbles from the submerged cluster. **a** appearance of large bubble on the cluster for brown sand (left) and green sand (right), **b** release of large bubbles from the cluster, before release, after release, view from above water surface, view from below water surface (note the clear appearance of the bubbles), **c** release of the last bubble from the cluster, before release, after release, view from above water surface, view from below water surface (note the particles attached on the bubble)

smaller and had a few sand particles that partially covered the bubble surface. The bubble burst almost instantly upon reaching the water surface. For the green sand, the last air bubble was also smaller in size; however, the fine sand particles covered the entire bubble surface. The bubble remained afloat just under the water surface (Fig. 6c) and lasted for over 1 hour before bursting.

We observed that the larger air bubbles (diameter = 4–6 mm) were released at about equal time intervals, which was 12 ± 3 min for the green sand clusters and 60 ± 4 min for the brown sand particles (except for the very last bubble). The size of the air bubbles released were about the same with no noticeable differences in bubble diameters between those released from the brown sand and green sand clusters (Fig. 6a). Between 5 and 6 large bubbles were released from the submerged cluster until all the particles were declustered. The release of the larger air bubbles from the submerged aggregate at about equal time intervals indicate that the rate of gas bubble mobilization and coalescence control the particle declustering rate. Because the coalescence of gas bubbles occurred at the upper central part (due to hydrostatic effects) of the submerged aggregate, the rate of bubble release is controlled by the ability of the micobubbles to coalesce with the larger gas bubble. This rate is correlated with the surface area of the central bubble where the microbubbles interact with the larger bubble (i.e., independent of the size of the remaining aggregate).

During our experiments with brown sand, stability of the clusters formed with different size particles did not differ significantly. Similarly, there were no significant differences in the stability of the submerged green sand clusters that were formed with different size particles. However,

stability of the brown sand clusters was significantly higher than those formed with the green sand. We relate the longer release time of the large air bubbles from the brown sand clusters to the existence of nano and micro bubbles on the surface of brown sand particles due to higher surface roughness. Presence of nanobubbles (due to surface roughness) enhances attachment of the air bubbles to the solid surfaces [28]. In our case, the existence of nanobubbles could explain the higher residence time of gas micro gas bubble within the interparticle pore space that resulted into longer release time of the larger air bubbles from the brown sand clusters. Moreover, pinning of nanobubbles, and, thus, facilitated stability of microbubbles, exists on rough surfaces [5, 10, 29].

7 Declustering characteristics by capillary effects and bubble coalescence

The limiting mass transfer area during the bubble formation depends on the number of particles surrounding the central bubble (that is subsequently released) in the submerged cluster. The central bubble moved gradually towards the top of the cluster and was released when about ½ of the bubble was exposed to water phase. Assuming at the time of release and assuming ½ of the bubble interfacial area is immersed in the cluster (the other ½ of the area is exposed to water phase), the bubble area in contact with the cluster (A_e) before release can be estimated as:

$$A_e = A_b\varepsilon/2 \tag{8}$$

Where A_b is total bubble area, and ε is the void fraction. The valued of both parameters (A_b and ε) were determined experimentally. Then, the average number of particles surrounding the bubble (n) can be estimated as follows:

$$n = \frac{A_e}{\pi r_p^2} \tag{9}$$

where r_p is the particle radius. The area through which the intercapillary gas bubbles are transferred and coalesce with the large bubble, or the effective capillary area (A_{eff}) can be estimated as:

$$A_{eff} = \frac{A_e}{n} \tag{10}$$

Assuming the particles are in speherical shape, then the effective capillary radius (r_{eff}) can be estimated as follows:

$$r_{eff} = (A_{eff}/\pi)^{0.5} \tag{11}$$

The rate of capillary volume displacement (r_c) can be estimated from the experimentally determined volume of the air bubble released (V_b) and the time interval between release of two consecutive bubbles (t) as follows:

$$r_c = V_b/t = \left(\frac{4}{3}\pi r_b^3\right)/t \tag{12}$$

Where r_b is the radius of the bubble released.

The apparent limiting bubble velocity during coalescence (v_{cr}) can be estimated by:

$$v_{cr} = (V_b/t)/A_e \tag{13}$$

Using the experimentally determined mass of cluster (m_c) and individual particle mass (m_p), the total number of particles in the cluster (n_{cl}) can be estimated as follows:

$$n_{cl} = m_c/m_p \tag{14}$$

Then, the particle declustering rate (r_d) (as number of particles per unit time) can be estimated as:

$$r_d = n_{cl}/t_d \tag{15}$$

Where n_{cl} is the total number of particles in the cluster (determined experimentally) and t_d is the total declustering time (determined experimentally).

Experimentally determined characteristics of the particles and the estimated cluster stability parameters for both green sand and brown sand particles are compared in Table 2. The experimental observations showed that declustering rate is highly dependent on the mobility and coalescence of the microbubbles in the submerged cluster. It was also observed that particle surface roughness had a significant effect on the entrapment as well as mobility of the microbubbles in the intercapillary space.

Numerical analyses of stability conditions for interaction of two air bubbles in liquid phase show that at surface tension values over 70 mN/m coalescence occurs on approach [3]. However, coalescence does not occur on approach in liquids with surface tensions less than 60 mN/m. The surface tension of water (72.86 ± 0.05 mN/m at 20 °C) allows coalescence at very small approach velocities (i.e., creep coalescence). During the experiments, it was observed that microbubbles moved towards the center of the cluster where they coalesced with the larger bubble at very small approach velocities that were calculated as 1.30×10^{-3} m/s for the green sand clusters and 5.72×10^{-5} m/s for the brown sand clusters.

8 Dimensionless numbers

For comparison of the relative magnitudes of the dominant forces on the cluster behavior, the magnitudes of the Bond number (Bo) and Capillary number (Ca) were calculated. The Bo relates to the ratio of the gravitational forces to

Table 2 Comparison of characteristics of the sand particles used and estimated clustering and declustering parameters of the submerged particle clusters

Parameter	Determination method	Green sand	Brown sand
Floating cluster			
Particle radius	r_p (measured)	1.65×10^{-4} m	3.65×10^{-4} m
Cluster mass (floating, max)	m_c (measured)	5.74 g	4.70 g
Cluster radius (floating, max)	R_{cm} (measured)	0.013 m	0.012 m
Average cluster perimeter	$2\pi R_{cm}$ (measured)	0.0816 m	0.0754 m
Cluster weight/cluster perimeter	$m_c g/(2\pi r_{cm})$	0.715 Nm^{-1}	0.631 Nm^{-1}
Submergence angle	θ (measured)	65°	55°
Cos θ		0.4226	0.5736
Particle cohesion coefficient (Particle clustering coefficient)	$P_{cc}=(m_c g)/(2\pi R_{cm}\gamma_{vl})$	9.57	8.49
Submerged cluster			
Cluster radius (floating, max)	R_{cm} (measured)	0.013 m	0.012 m
Cluster volume (assuming half sphere)	V_{cl} (calculated)	4.60×10^{-5} m^3	3.62×10^{-6} m^3
Gas bubble release time	t (measured)	720 s	3600 s
No of bubble released	n_b	5-6	5-6
Total declustering time	t_d (measured)	3960 s	19,800 s
Radius of gas bubble released	r_b (measured)	0.0025 m	0.0025 m
Volume of gas bubble released	$V_b=\left(\frac{4}{3}\pi r_b^3\right)$	6.54×10^{-8} m^3	6.54×10^{-8} m^3
Void fraction of aggregate	ε (from data)	0.82	0.76
Interfacial area of bubble released	$A_b=\left(4\pi r_b^2\right)$	7.85×10^{-5} m^2	7.85×10^{-5} m^2
Bubble coalescence area	$A_e=A_b\,\varepsilon/2$	3.22×10^{-5} m^2	2.98×10^{-5} m^2
Average number of particles surrounding central bubble at time of release	$n=\frac{A_e}{\pi r_p^2}$	376	71
Effective capillary area (equivalent radius of voids)	$A_{eff}=\frac{A_e}{n}$	6.99×10^{-8} m^2	3.18×10^{-7} m^2
Effective capillary radius (equivalent radius of voids)	$r_{eff}=(A_{eff}/\pi)^{0.5}$	1.49×10^{-4} m	3.18×10^{-4} m
Effective radius/Particle radius	r_{eff}/r_p	0.904	0.872
Rate of capillary volume displacement	$r_c=V_b/t$	9.09×10^{-11} m^3/s	1.82×10^{-11} m^3/s
Apparent limiting bubble velocity during coalescence	$v_{cr}=(V_b/t)/A_e$	1.30×10^{-3} m^3/m^2 s	$5.72x10^{-5}$ m^3/m^2 s
Number of particles in cluster	$n_{cl}=m_c/m_p$	223,000–350,000	6000–7500
Particle declustering rate	$r_d=n_{cl}/t_d$	56–91 particles/s	0.30–0.38 particles/s

interfacial forces on the particles in the cluster and it is expressed as follows:

$$Bo = \Delta\rho\, g\, r_{eff}^2/\gamma_{vl} \tag{16}$$

For Bo values that are significantly smaller than 1, it is considered that interfacial forces are more significant than gravitational forces during liquid flow. The estimated Bo values were significantly smaller than 1 for both types of particles used (brown sand $Bo=1.38\times10^{-2}$ and green sand $Bo=3.03\times10^{-3}$), which implies strong interfacial effects in comparison to the gravitational effects on the cluster behavior (Table 3). The larger values of Bo for the brown sand cluster is also due to the higher density of the brown sand particles (1700 kg/m^3) and the larger estimated effective radius (3.18×10^{-4} m) in comparison to the green sand particles with relatively lower density (1550 kg/m^3) and smaller estimated effective radius (1.49×10^{-4} m).

Table 3 The bond and capillary numbers calculated for the submerged particle clusters

Dimensionless number	Green sand	Brown sand
Bond number = gravitational force/interfacial force $Bo=\Delta\rho\, g\, r_{eff}^2/\gamma_{vl}$	3.03×10^{-3}	1.38×10^{-2}
Capillary number = viscous force/interfacial force $Ca=\eta\, v_{cr}/\gamma_{vl}$	1.06×10^{-5}	7.06×10^{-7}

The Ca relates to the ratio of the viscous forces to interfacial forces on the cluster. The Ca values smaller than 10^{-5} indicate that capillary forces dominate the flow conditions

in the porous medium. For calculation of Ca, apparent limiting bubble coalescence rate (v_{cr}) was used as the liquid velocity in the cluster as follows:

$$Ca = \eta v_{cr} / \gamma_{vl} \quad (17)$$

Comparison of the Ca values show that the brown sand clusters exhibited significantly higher interfacial forces, thus smaller Ca in comparison to that for the green sand clusters (green sand $Ca = 1.06 \times 10^{-5}$ vs brown sand $Ca = 7.06 \times 10^{-7}$) (Table 3). The movement of water within the brown sand clusters were significantly slower in comparison to that in the green sand clusters (1.30×10^{-3} for green sand clusters vs 5.72×10^{-5} m/s for brown sand clusters). The low Ca values indicate that interfacial surface forces (between water and cluster) or capillary forces dominate the viscous forces during the declustering process.

9 Discussion

The clustering of granular particles occur when three phases are in contact (i.e., solid particle, water, air). If one of the phases is not present, there is not adequate force to keep the particles together. For example, if there is no liquid, particles remain loose (due to absence of liquid bridges). Similarly, if there is no air (or gas phase) in the cluster, the particles would form slurry (due to absence of gas bridges) (Fig. 7).

Initially, we tried to use Washburn equation to estimate the capillary radius. In the submerged particle clusters, hydrostatic pressure and counteracting forces mobilize the air in the capillaries towards the center of the cluster. The rate of displacement of gas with water occurs at much slower rates in comparison to the capillary rise phenomena where Washburn equation is applicable. The submerged cluster is not in cylindrical shape, but almost in the shape of a half sphere. As water enters from the outside of the cluster (large transport area), the gas bubbles move towards the upper central section of the cluster where they coalesce with the larger cluster. Thus, the gas transport area becomes smaller as the bubbles move towards the center of the cluster (where they coalesce). The attempts to use the Washburn equation to estimate the capillary radius resulted into unreasonably small capillary radius (near atomic size). Therefore, the Washburn equation that is used to describe the capillary transport of water in granular materials is not appropriate for analyzing the wetting/declustering process occurring in the submerged hydrophobic granular clusters in water (Fig. 7). The transport phenomenon of water for the case of water in granular materials is very different from that occurring in granular clusters in water where hydrostatic forces also into play for mobilization of air bubbles.

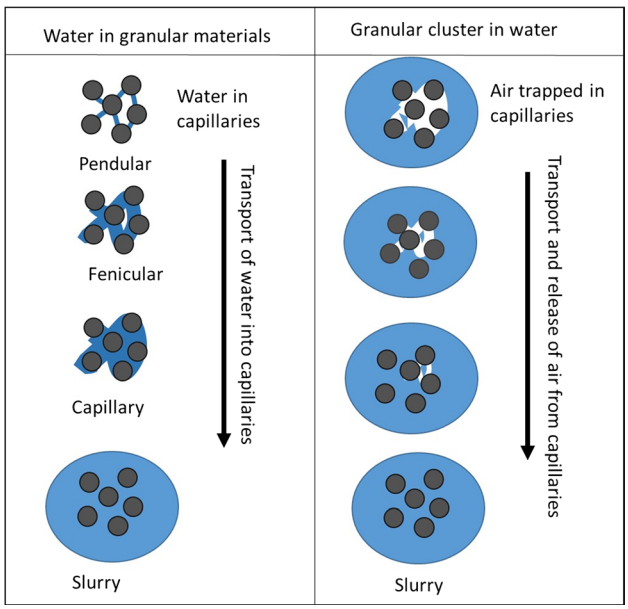

Fig. 7 Comparison of different particle-water-gas phase conditions for liquid in granular materials and granular materials in liquid

Based on the experimental data, the estimated ratios of the effective radius to particle radius for the submerged green and brown sand clusters were 0.904 and 0.879, respectively. In other words, the effective capillary radius in the submerged clusters is about 90% of the particle radius.

It was observed that the particle size affects the spreading tendency of the particles on the water surface. Smaller particles exhibit higher spreading tendency than the larger particles due to relatively larger effect of surface forces (e.g., surface charges) in comparison to the gravitational effects.

Hydrostatic pressure plays a role in mobilizing the air towards the center and upper portion of the cluster and eventually for the release of the air bubbles from the cluster due to buoyancy effects. We have conducted the experiments in 50-mL beakers, thus, the effect of hydrostatic pressure was small. We have also conducted additional experiments to explore the effect of depth of water column on the declustering behavior using 1-L beakers. Again, the water depth was not sufficiently high to observe the effect of hydrostatic pressure on the bubble release and declustering characteristics. The declustering phenomenon is rather complex as the bubble size is also affected by the hydrostatic pressure. Experimentally, we were able to measure the bubble sizes more accurately when the water depth was small so that the size of the bubbles released did not change in size significantly as they ascended towards the water surface.

It is important to note that the cluster of particles exhibits different interfacial and wetting characteristics from those of the individual particles that make up the cluster. Particle shape, particle size, arrangement of the particles at the cluster-water interface and void fraction of the cluster result in different wetting characteristics at the cluster-water interface

from those of the solid material of the particles. In other words, a cluster that is formed from granular quartz particles exhibits different interfacial and wetting characteristics from those exhibited by a quartz surface (or a single quartz particle).

The larger the amount of gas trapped between the particles and on the particle surface, the larger would be the floating cluster mass (before submergence) due to the increased effects of buoyancy forces. The higher the hydrophobic tendency of the particles, the smaller the wetting angle θ would be to avoid wetting (or submerging), thus, yielding a larger cluster radius (but shallower sac) while allowing larger amount of particles to remain afloat (Fig. 5a). On the other hand, due to the gravitational and buoyancy effects (i.e., higher density of particles than that of water), the particle cluster gradually submerges into the water while still remaining afloat. For the hydrophobic particles, the air trapped between the particle surface and water phase as well as air trapped inside the cluster, prevent the particles from being wetted easily. Because of both the larger cluster diameter (0.013 m) the green sand clusters had about 0.00574 kg total particle mass before submergence although their bulk density was smaller (1500 kg/m^3) and the cluster had larger submergence angle (65°). The brown sand clusters were 0.012 m diameter and carried about 0.0047 kg total particle mass before submergence due to the higher bulk density (1700 kg/m^3) and smaller submergence angle (55°).

10 Conclusions

Hydrophobic granular particles form clusters when they interact with water. Particle clustering appears to occur by entrapment of the gas bubbles between the particles as well as micro and nanobubbles that remain attached on the particle surface. Presence of nano and micro scale gas bubbles reduce the contact are of the particles with water. Hence, the submerged hydrophobic particles form clusters which allows the aggregated particles to remain stable for extended periods of time. The use Bo and Ca do not provide adequate insight neither for clustering tendency nor cluster stability of granular particles for evaluating the behavior of hydrophobic granular particle clusters.

Experimental observations showed there are significant differences in (1) the clustering tendency of granular particles and (2) the stability of the submerged clusters in water. Clustering tendency depends on the surface tension characteristics (or spreading tendency) of the particles on the water surface. Particle cohesion factor was defined for comparing clustering tendency during interaction of particles with water.

The cluster of particles exhibits different interfacial characteristics from those of the individual particles that make up the cluster. The cluster stability is highly dependent on surface roughness of the particles that affects the ability of the microbubbles to mobilize and coalesce within the submerged cluster. The experimental results showed that surface characteristics (i.e., roughness) affect the rate of creep coalescence of the gas phase and declustering rate of granular particles in water.

Acknowledgements Partial support for this research has been provided by Postdoctoral Fellowship funding by Florida International University.

Compliance with ethical standards

Conflict of interest The authors declare that they have no conflict of interest.

Informed consent Informed consent was obtained from all individual participants included in the study.

References

1. Attard, P., Moody, M.P., Tyrrell, J.W.G.: Nanobubbles: the big picture. Phys. A **314**, 696–705 (2002)
2. Ball, P.: Chemical physics: how to keep dry in water. Nature **423**, 25–26 (2003)
3. Berry, J.D., Dagastine, R.R.: Mapping coalescence of micron-sized drops and bubbles. J. Colloid Interface Sci. **487**, 513–522 (2017)
4. Ducker, W.A.: Contact angle and stability of interfacial nanobubbles. Langmuir **25**, 8907–8910 (2009)
5. Fritzsche, J., Peuker, U.A.: Modeling adhesive forces caused by nanobubble capillary bridging. Colloids Surf. A Physicochem. Eng. Asp. **509**, 457–466 (2016)
6. Hampton, M.A., Nguyen, A.V.: Nanobubbles and the nanobubble bridging capillary force. Adv. Colloid Interface Sci. **154**, 30–55 (2010)
7. Kralchevsky, P., Nagayama, K.: Particles at Fluid Interfaces and Membranes. Elsevier, Amsterdam (2001)
8. Liu, B., Lange, F.E.: Pressure induced transition between superhydrophobic states: configuration diagrams and effect of surface feature size. J. Colloid Interface Sci. **298**, 899–909 (2006)
9. Ljunggren, S., Eriksson, J.C.: The lifetime of a colloid-sized bubble in water and the cause of the hydrophobic attraction. Colloids Surf. A Physicochem. Eng. Asp. **129–130**, 151–155 (1997)
10. Liu, Y., Zhang, X.: Nanobubble stability induced by contact line pinning. J. Chem. Phys. **138**, 014706 (2013)
11. Marmur, A.: The lotus effect: superhydrophobicity and metastability. Langmuir **20**, 3517–3519 (2014)
12. Meyer, E.E., Rosenberg, K.J., Israelachvili, J.: Recent progress in understanding hydrophobic interactions. PNAS **103**, 15739–15746 (2006)
13. Myshkis, A.D., Babskii, V.G.: Low-Gravity Fluid Mechanics Mathematical Theory of Capillary Phenomena. Springer, Berlin (1987)
14. Nguyen, T.H., Hapgood, K., Shen, W.: Observation of the liquid marble morphology using confocal microscopy. Chem. Eng. J. **162**, 396–405 (2010)

15. Parker, J.L., Claesson, P.M., Attard, P.: Bubbles, cavities, and the long-ranged attraction between hydrophobic surfaces. J. Phys. Chem. **98**, 8468–8480 (1994)
16. Patankar, N.A.: Mimicking the lotus effect: influence of double roughness structures and slender pillars. Langmuir **20**, 8209–8213 (2004)
17. Petkov, P., Radoev, B.: Statics and dynamics of capillary bridges. Colloids Surf. A Physicochem. Eng. Asp. **460**, 18–27 (2014)
18. Princen, N.M.: The Equilibrium Shape of Interfaces, Drops and Bubbles. Rigid and Deformable Particles at Interfaces. In: Matijievich, E. (ed.) Surface and Colloid Science. Willey, New York (1969)
19. Radoev, B., Ivanova, I.T., Petkov, P.: Capillary bridge: transition from equilibrium to hydrodynamic state. Colloids Surf. A Physicochem. Eng Asp. **505**(2016), 98–105 (2016)
20. Sharma, P., Deasgubpta, A.: Micro-mechanics of creep-fatigue damage in Pb-Sn solder due to thermal cycling—part I: formulation. Trans. ASME **124**, 292–297 (2002)
21. Steitz, R., Gutberlet, T., Hauss, T., Klosgen, B., Krastev, R., Schemmel, S., Simonsen, A.C., Findenegg, G.H.: Nanobubbles and their precursor layer at the interface of water against a hydrophobic substrate. Langmuir **19**, 2409–2418 (2003)
22. Sun, Y., Xie, G., Peng, Y., Xia, W., Sha, J.: Stability theories of nanobubbles at solid–liquid interface: a review. Colloids Surf. A Physicochem. Eng. Asp. **495**, 176–186 (2016)
23. Tyrrell, J.W.G., Attard, P.: Images of nanobubbles on hydrophobic surface and their interactions. Phys. Rev. Lett. **87**, 176104 (2001)
24. Van der Giessen, E., Tvergaard, V.: On cavity nucleation effects at sliding grain boundaries in creeping polycrystals. In: Wilshire, B., Evans, R.W. (eds.) Creep and Fracture of Engineering Materials and Structures, pp. 169–178. Elsevier, Swansea (1990)
25. Yang, S., Dammer, S.M., Bremond, N., Zandvliet, H.J.W., Kooij, E.S., Lohse, D.: Characterisation of nanobubbles on hydrophobic surfaces in water. Langmuir **23**, 7072–7077 (2007)
26. Zhang, X.H., Maeda, N., Craig, V.S.J.: Physical properties of nanobubbles on hydrophobic surfaces in water and aqueous solutions. Langmuir **22**, 5025–5035 (2006)
27. Zhang, X.H., Khan, A., Ducker, W.A.: A nanoscale gas state. Phys. Rev. Lett. **98**, 136101 (2007)
28. Zhang, X., Kumar, A., Scales, P.J.: Effects of solvency and interfacial nanobubbles on surface forces and bubble attachment at solid surfaces. Langmuir **27**, 2484–2491 (2011)
29. Zhang, X., Chan, D.Y.C., Wang, D., Maeda, N.: Stability of interfacial nanobubbles. Langmuir **29**, 1017–1023 (2013)
30. Zhu, Z.F., Jia, J.Y., Fu, H.Z., Chen, Y.L., Zeng, Z., Yu, D.L.: Shape and force analysis of capillary bridge between two slender structured surfaces. Mech. Sci. **6**, 211–220 (2015)